Cavity Ring-Down Spectroscopy of the Torsional Motions of 1,4-Bis(phenylethynyl)benzene

Stuart J. Greaves, Emma L. Flynn, Emma L. Futcher, Eckart Wrede,* Donocadh P. Lydon, Paul J. Low, Simon R. Rutter, and Andrew Beeby

University of Durham, Department of Chemistry, South Road, Durham DH1 3LE, U.K.

Received: August 8, 2005; In Final Form: December 16, 2005

The torsional motions of jet-cooled 1,4-bis(phenylethynyl)benzene (BPEB), a prototype molecular wire, were studied using cavity ring-down spectroscopy in the first UV absorption band (316−321 nm). The torsional spectrum of 1,4-bis(phenylethynyl)-2,3,5,6-tetradeuteriobenzene was also recorded in the gas phase. Both spectra were successfully simulated using simple cosine potentials to describe the torsional motions. The ground-state barrier to rotation was estimated to be 220−235 cm^{-1}, which is similar to that of diphenylacetylene (tolane). Complementary DFT calculations were found to overestimate the torsional barrier.

1. Introduction

Molecular and polymeric materials based upon the phenylethynyl motif are a source of considerable interest, much of which arises from the rigid molecular structure[1] and the extended delocalized π-electron system that these systems offer.[2] The combination of these properties with the variable substitution patterns that can be employed around the phenyl ring system has led to a rapid development of a wide-range of shape-persistent molecular architectures,[3] luminescent and electroluminescent materials[4−6] and Langmuir−Blodgett films for OLED applications,[7] organic semiconductors,[8] and solid materials that can support remarkably well-ordered micrometer features through thermal cross-linking via multiple [3+2] cycloaddition reactions.[9]

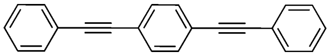

The elementary 1,4-bis(phenylethynyl)benzene (BPEB, **1**) framework has also attracted considerable attention as a potential “molecular wire”.[10−15] The observation of bistable conductive states of such systems, which could be switched by applied potentials[15] and displayed negative differential resistance in metal-molecule-metal devices,[16,17] has provoked immense debate about the potential for such compounds to find application in true molecular electronic devices. The majority of attempts to rationalize these observations have been directed toward the role of conformational changes in the molecular backbone, specifically the role the relative intramolecular orientation of the aromatic rings might play in disrupting the delocalized π-framework.[18−22] However, a variety of other possibilities have also been suggested, including variation in the coupling between the molecule and the electrode,[23] and variation in the localization of the frontier orbitals.[24]

Computational methods have been used to examine the frontier orbitals of BPEB, and its derivatives, in both idealized twisted and planar configurations. These molecular orbital (MO) pictures show the π-orbitals to be delocalized across the whole molecule in the planar configuration and isolated on the central ring in the twisted configuration.[25,26] The different methodologies used for these calculations appear to have very little effect upon the MO picture, but the energies of the orbitals are markedly different.[26] It has been claimed that there is a 500 times change in conductance on rotation of the middle ring, from planar to perpendicular, of BPEB.[27]

Studies on systems with restricted rotation about the principal axis demonstrate the influence conformational factors can exert on the electronic structure of these materials.[28−32] The low-energy barrier to rotation about the C(sp-ethynyl)−C(sp^2-aryl) bonds in the ground state of oligomeric phenylethynyl materials makes engineering control of such conformational properties in unrestricted systems exceedingly difficult. To the best of our knowledge, no one has yet succeeded in measuring this ground-state barrier, although variable temperature electronic absorption, excitation and luminescence spectroscopy have been used to demonstrate that the rotational barrier is greater in the first excited state.[33] Further investigation of the S$_1$ state by resonance/nonresonance Raman spectroscopic results showed that the C(sp)−C(sp) bonds retain triple bond order with no evidence for any significant cumulenic/quinoidal character.[34]

The absorption spectrum of BPEB in cyclohexane solution shows a series of partially resolved absorption bands between 250 and 350 nm, with a sharp band edge at the red end of the absorption profile.[33] Though the results of solution based spectroscopic studies give valuable insight into the character of the excited state of BPEB,[33] they lack detailed information about the important torsional motion of the molecule in either the ground or excited states.

To resolve the torsional transitions experimentally, the spectral congestion (caused by the large number of normal modes and solvent effects) needs to be radically reduced, e.g., by cooling the gaseous sample in a supersonic jet expansion.

Similar methods have been used together with fluorescence spectroscopy to measure the torsional motion in diphenylacetylene (tolane).[35,36] The ring twisting barrier was found to be 202 cm^{-1} in the ground state and $\approx$1600 cm^{-1} in the excited state. However, the markedly different structures of its close-lying excited states make tolane unsuitable as a model for BPEB, and thus longer poly(phenylethynylene) (PPE) molecules.[37]

Zheng et al. have used a lumped-inertia technique to predict the vibrational frequencies of the torsional modes of PPEs.[38] For tolane, the two-ring PPE, the calculated value for the

---

* To whom correspondence should be addressed. E-mail: eckart.wrede@durham.ac.uk.

10.1021/jp054426h CCC: $33.50

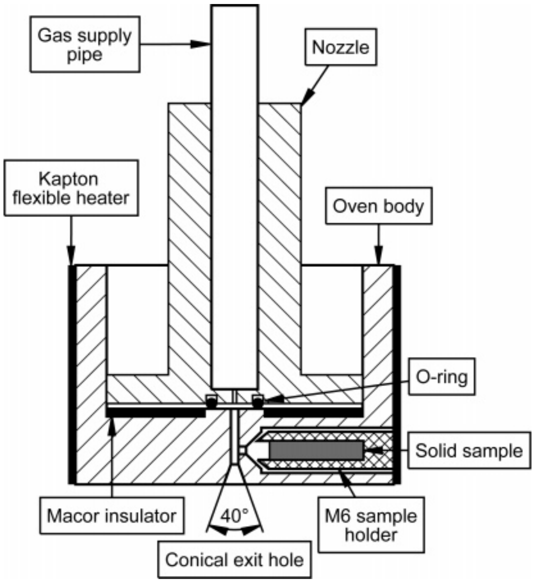

Figure 1. Cross section of the sample oven and nozzle assembly. The solid sample is stored in a hollow M6 screw within the cylindrical oven (copper). The 40° cone at the end of the 1 mm exit channel enhances the focusing and cooling of the molecular beam. The nozzle is thermally isolated from the oven via a ceramic disk (Macor).

torsional frequency, 16 cm^{-1}, is in good agreement with the experimental value of 17 cm^{-1},[35] and the predicted values for the two BPEB torsional frequencies are 13.2 and 19.4 cm^{-1}. Zheng et al. found that the force constants used for the twist of adjacent rings were invariant with the length of the PPE, but the force constants for longer range interactions (next-nearest neighbors) are increased with length, highlighting the effect of the extended conjugation in these systems.[38]

In this paper we present the first measurement of the torsional potentials of BPEB, using the highly sensitive cavity ring-down spectroscopy (CRDS) technique. The remainder of this article is structured as follows: section 2 describes the experimental setup; section 3 contains the experimental results; the data are analyzed and discussed in section 4; section 5 gives details of the complementary DFT calculations; conclusions are summarized in section 6.

2. Experiment

2.1. Molecular Beam Apparatus. The description of the key features of the experimental setup is given here, and additional detail is available in the Supporting Information (section S1).

The molecular beam was generated by a pulsed, unskimmed nozzle (Parker Instrumentation, General Valve Series 9, 0.5 mm orifice, with IOTA ONE pulse driver) using argon carrier gas. The nozzle was mounted on a *x*, *y*, *z*-adjustable stage on the vertical axis of the vacuum chamber (Supporting Information, Figure 1S). Figure 1 shows the sample oven adapted from a design used to study biological molecules in the gas phase.[39,40] The oven is a copper cylinder with a central 1 mm diameter (exit) channel directly mounted to the nozzle. A second 1 mm diameter channel intersects at right angles to the first and leads to a M6 tapped bore in the side of the oven, which houses a hollow M6 screw used to hold the sample. A ceramic disk (Macor) reduces the thermal load on the nozzle from the oven, which is heated by a flexible heater (Omegalux, Kapton flexible heater). The BPEB vapor is “caught” in the exit channel and seeded into the gas pulse, which expands and cools after leaving the oven. A 3 mm deep 40° cone at the exit of the oven is used to spatially focus the beam expansion and enhance cooling, as suggested by Even et al.[41] The divergence of the molecular beam was ≈20° (full width half-maximum, fwhm), estimated from BPEB deposits in the chamber.

A retractable fast ionization gauge (Beam Dynamics Inc., FIG-1) was mounted 3 cm below the oven exit to allow nozzle adjustment and monitoring of the molecular beam in situ. Short, intense pulses (fwhm ≈200 μs) were obtained. The FIG was also used to ensure correct temporal overlap of the molecular beam and laser pulses.

The chamber was evacuated to approximately 10^{-7} mbar by a diffusion pump (BOC Edwards, Diffstak CR100/300, 230 L s^{-1}), which was backed by a rotary vane pump (Varian, DS202, 8.3 $\text{m}^3\ \text{h}^{-1}$). The pressure in the chamber was monitored using a Bayard-Alpert ionization gauge (Leybold, Ionivac ITR90).

2.2. Cavity Ring-Down Setup. The CRDS method[42−44] measures the rate of absorption of a light pulse confined in a stable optical cavity formed by two highly reflective mirrors (reflectivity, $\mathscr{R} > 99.9\%$). A short laser pulse coupled into the cavity is reflected back and forth and, every time the light is reflected, a small fraction ($\approx 1 - \mathscr{R}$) “leaks out”, leading to exponential decay of the pulse in the cavity. The decay time (ring-down time, RDT) is determined by measuring the time dependence of the intensity of light leaking out of the cavity.

Light absorbed by the sample between the mirrors will increase the decay of light and hence reduce the RDT. The molecular absorption coefficient, α, can be determined using

$$1/\tau' = 1/\tau + c\alpha \tag{1}$$

where τ' is the RDT with sample, τ is the RDT of the empty cavity and *c* is the speed of light.[43] Because of the molecular beam used in this experiment, eq 1, which assumes constant sample density over the whole length of the cavity, cannot be applied directly. Although the density in the beam is not known, relative absorptions can still be measured.

Two highly reflective cavity mirrors (Layertec, plano-concave $R = 1$ m, $\mathscr{R} \geq 99.9\%$ between 330 and 340 nm, diameter 7.75 mm) were mounted at a distance of 77 cm on knife-edge bellows on the horizontal axis of the vacuum chamber as windows. Mirror positions were adjusted by micrometer screws (Thorlabs) in a configuration designed to replicate a kinematic optical mount. The distance between the exit of the sample oven and the cavity axis was optimized at 8 mm.

2.3. Laser System and Data Acquisition. The second harmonic of a Nd:YAG laser (Continuum, Surelight I-10, pulse length 5 ns, repetition rate 10 Hz) was used to pump a dye laser with second harmonic generation and Pellin-Broca wavelength separator (Sirah, Cobra Stretch). The dye laser was operated with DCM dye (in methanol) and only the oscillator and preamplifier were used. The accessible wavelength range of the doubled light was 301−330 nm with the pulse energy limited to ≤0.4 mJ at 320 nm by reducing the Nd:YAG pump power to avoid overload of the photomultiplier tube (PMT) detector. The bandwidth of the doubled laser light was 0.08 cm^{-1}.

A spatial filter consisting of a lens (plano-convex, 100 mm), pinhole (diameter 100 μm), and lens (plano-convex, 50 mm) was used to ensure all light entering the cavity had a Gaussian beam profile, as described by Lee et al.[45] A 750 mm plano-convex lens was placed 37 mm in front of the cavity entrance mirror to couple the laser light efficiently into the TEM_{00} mode of the cavity (see Supporting Information section S1.2 for details). The polarization of the laser light entering the cavity was vertical.

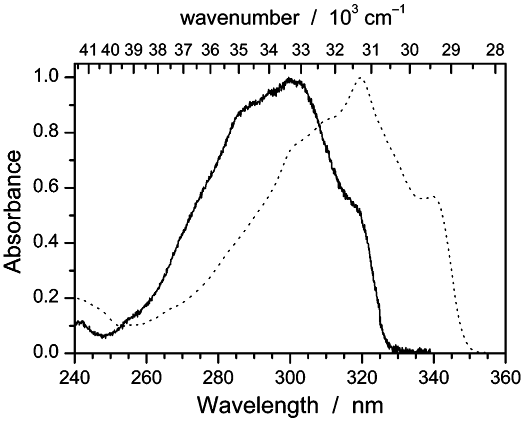

Figure 2. Low-resolution ($\Delta\lambda = 0.2$ nm) UV−vis spectra of BPEB in cyclohexane solution (room temperature, dotted line)[33] and in the gas phase (110−130 °C, solid line). Both spectra are normalized to aid comparison.

The transmitted light through the output mirror of the cavity was detected by a photomultiplier tube (Hamamatsu, PMT Model R1463; 20% maximum quantum efficiency at 350 nm). The PMT was coupled to a digitizing oscilloscope (LeCroy, Waverunner LT584), which was connected to a PC via a IEEE-488 interface (National Instruments, PCI-GPIB). The PC was used for experimental control and data acquisition using a customized version of a LabVIEW (National Instruments) program developed at the University of Bristol.[46] The program normalized the data by subtracting the baseline (region of trace before the ring-down event corresponding to no laser light in cavity) from the exponential curve. A least-squares fit was performed on the natural logarithm of these data to obtain the gradient, the inverse of which is the ring-down time. The least-squares fit was also used to calculate the mean-squared error (MSE) of the exponential fit, which was compared with a user set value of maximum MSE so that nonexponential curves could be excluded from data acquisition.

Prior to scans, the cavity mirrors were aligned to achieve simultaneously maximum ring-down time, low shot-to-shot noise and minimal deviation from an exponential decay curve. The temporal overlap of the molecular beam and laser pulses was controlled using a multichannel delay generator (University of Bielefeld, Physics Department). Both temporal and spatial overlap of the molecular and laser beams were optimized prior to scans to maximize signal levels.

2.4. Synthesis. The synthesis of BPEB has been described previously.[33] 1,4-bis(phenylethynyl)-2,3,5,6-tetradeuteriobenzene, from here on known as D-BPEB, was synthesized using the previously reported method by Lydon et al. starting from perdeuteriobenzoquinone[47] and full details are given in the Supporting Information (section S1.3).

3. Results

3.1. High-Temperature Spectra of BPEB. The gas-phase spectrum of BPEB, which has not been reported previously, has been measured to investigate the wavelength range required for the CRDS experiment. A sample of BPEB was placed in a cylindrical glass cell with UV-grade fused silica windows (Comar). The cell was evacuated to 10^{-2} mbar and heated to temperatures between 110 and 130 °C using flexible heaters (Omegalux, Kapton flexible heater) to produce BPEB vapor. No evidence of decomposition was found after heating. The gas-phase spectrum was recorded with a UV−vis spectrometer (Unicam, UV-4) and is shown in Figure 2 together with a spectrum of BPEB in cyclohexane solution at room temperature.[33]

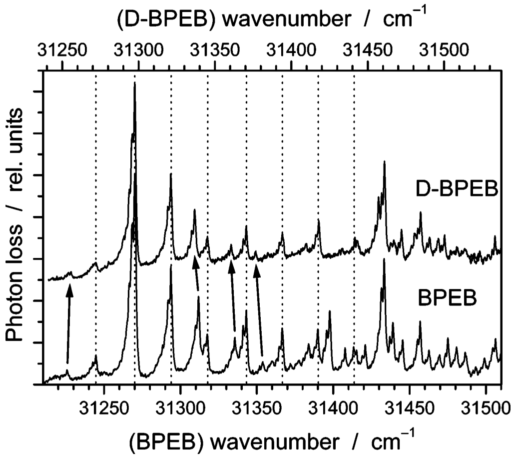

Figure 3. Cavity ring-down spectra of BPEB and D-BPEB. The wavenumber axis for the latter has been shifted to line-up the band heads of both spectra and a vertical offset has been added to ease comparison. The peaks due to the antisymmetric mode have the same relative spacing, and peaks with a contribution from the symmetric mode are shifted by the deuteration of the central ring (indicated by arrows).

The solution phase spectrum shows a series of partially resolved absorption bands between 250 and 350 nm. As cyclohexane is a nonpolar solvent, the solution and gas-phase spectra are of similar shape, although the latter was recorded at a much hotter gas temperature. Due to solvent effects, however, the gas-phase spectrum is blue shifted by about 20 nm compared to the spectrum in solution. Unfortunately, this blue shift meant that the first absorption band did not coincide with the wavelength range of highest reflectivity of the mirrors. High-quality CRD spectra could still be recorded (see below); however, some loss of sensitivity was inevitable.

3.2. Spectra of Jet-Cooled BPEB. “Empty” cavity scans were recorded before or after each CRD spectrum of BPEB. The firing of the nozzle was mistimed such that the empty cavity ring-down time, τ in eq 1, could be determined at otherwise identical conditions.

Optimized experimental conditions for the recording of cold BPEB spectra were found to be 145−155 °C oven temperature, 4−5 bar Ar stagnation pressure, and ≈200 μs gas pulse length (fwhm), resulting in a chamber pressure between 1×10^{-4} and 5×10^{-4} mbar.

The spectrum of BPEB over the usable spectral range of the experiment is shown in comparison with the spectrum of D-BPEB in Figure 3. At lower frequencies, despite the increase in ring-down time due to better mirror reflectivity, no further transitions were observed. At higher frequencies the ring-down time decreased until any further transitions were indistinguishable from the noise floor. No features attributable to impurities were observed, and all spectra were reproducible, within the limits of experimental stability.

The relative peak intensities in the spectra depend on the torsional temperature, whereas the width of the peaks seemed to be correlated with the cooling of rotations and nontorsional vibrational modes in the beam. Depending on the beam temperature achieved, the peak shape changed from spectrum to spectrum; however, it was of constant shape within each spectrum.

3.3. Wavelength Calibration. A room-temperature cavity ring-down spectrum of iodine vapor, using a simple tubular cavity, was recorded to check the calibration of the fundamental

TABLE 1: Normal Torsional Modes of BPEB[a]

mode	eigenvalues $-\omega^2$	eigenvectors		
		C_1	C_2	C_3
rotation	0	1	1	1
antisymmetric (as)	$-(k^{(1)} + 2k^{(2)})/I_{\mathrm{end}}$	−1	0	1
symmetric (s)	$-k^{(1)}(2I_{\mathrm{end}} + I_{\mathrm{mid}})/I_{\mathrm{end}}I_{\mathrm{mid}}$	1	$-2I_{\mathrm{end}}/I_{\mathrm{mid}}$	1

[a] ω: vibrational angular frequency. C_i: amplitude of torsional oscillation of ring i. $k^{(1)}$, $k^{(2)}$: force constants between adjacent rings and between next-nearest neighbors, respectively. I_{end}, I_{mid}: moments of inertia of the outermost and central rings, respectively.

TABLE 2: Simulation Parameters for BPEB and D-BPEB Spectra

parameter	BPEB	D-BPEB
I_{end}/amu Å^2	88.9036	
I_{mid}/amu Å^2	89.0536	107.560
I_{red} (as)/amu Å^2	88.9036	
I_{red} (s)/amu Å^2	29.6688	33.5093
$V_{\max}$ (as)/cm^{-1}	222.82 ± 1.7[a]	
$V_{\max}$ (s)/cm^{-1}	232.76 ± 1.4[a]	
excited-state scaling factor (as)	8.01 ± 0.01	7.93 ± 0.01
excited-state scaling factor (s)	8.01 ± 0.01	7.96 ± 0.01
T_{torsion}/K	37 ± 1	36 ± 1
$00 \leftarrow 00$ band origin/cm^{-1}	31,269.7 ± 0.5	31,297.1 ± 0.5
additional progressions	position[b]/cm^{-1}	intensity[c]
BPEB 1	73.0	0.18
BPEB 2	127.6	0.17
BPEB 3	163.2	0.40
D-BPEB 1	73.5	0.07
D-BPEB 2	163.5	0.45

[a] Progression of error in ν_e; the spectra were simulated using five significant figures as listed. [b] Origin of additional progressions relative to position of $00 \leftarrow 00$ band. [c] Intensity of additional progressions relative to $00 \leftarrow 00$ intensity.

output of the dye laser. Iodine spectra were obtained over the wavelength range 632−641 nm and compared with simulations using the WI2 program by Western.[48] Relative line positions were accurate to ±0.05 cm^{-1} and absolute line positions between −0.1 and −0.4 cm^{-1}, well within the stated calibration limits of the laser.

4. Analysis and Discussion

4.1. Normal-Mode Analysis. Analysis of the twisting modes of BPEB follows the technique of Zheng et al.,[38] a method specifically designed for the torsional motion of PPEs. The vibrational analysis of BPEB can be simplified by modeling each phenyl ring as a rigid body with a "lumped inertia" equal to that of the ring and its attached hydrogens (or other symmetrically located substituents). The twisting modes are described as relative rotations of these inertias about the principal axis of BPEB, with adjacent inertias interacting with torsional force constants, k (which has units of energy). The normal-mode analysis is discussed in detail in Supporting Information section S2.

The resultant eigenvalue problem (Supporting Information, eq 14S) is solved for the eigenvalues, $-\omega^2$, and eigenvectors that are obtained in terms of the force constants, $k^{(1)}$ and $k^{(2)}$, and moments of inertia, I_j. For BPEB, the inertia of the outermost phenyl rings are identical, $I_{\mathrm{end}} = I_1 = I_3$. The inertia of the central ring, $I_{\mathrm{mid}} = I_2$, is similar, but not identical, to I_{end}, as the carbon−carbon bond lengths of the central ring are slightly different from those of the outer rings (see Table 2). The result of the normal-mode analysis is summarized in Table 1. If the force constant between a ring and its second-nearest neighbor, $k^{(2)}$, is not included in the eigenvalue calculation (i.e., only nearest-neighbor interactions are considered), the antisymmetric eigenvalue becomes $-\omega_{\mathrm{as}}{}^2 = -k^{(1)}/I_{\mathrm{end}}$. The eigenvalue of zero corresponds to the free rotation of the entire molecule around its z-axis. The motion of the rings in the antisymmetric and symmetric modes (with respect to the $\sigma(xy)$ mirror plane) is illustrated in Figure 4.

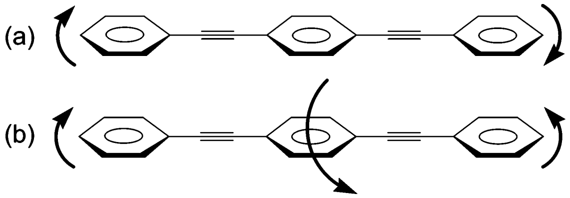

Figure 4. (a) Antisymmetric and (b) symmetric normal mode twists of BPEB.

4.2. Deuterated BPEB. Isotopic substitution is a well-known technique for the elucidation of complex spectra. The difference between the twisting motion of the symmetric and the antisymmetric modes is the participation of the central phenyl ring (see Figure 4). With the hydrogens on the central ring replaced with deuteriums, thus changing I_{mid}, transitions in the spectrum involving the symmetric twisting mode (and any other vibrations that move the middle ring) change their positions. Transitions involving exclusively antisymmetric torsions remain stationary. Some symmetric twisting transitions are identified by arrows in Figure 3.

4.3. Spectral Simulations. To simulate the BPEB spectrum, the torsional potentials of the two twisting modes, in both the ground and excited states, are required. The energy levels for these potentials give the line positions of the torsional transitions. The wave functions for each energy level are used to calculate the Franck−Condon factors, which, in combination with a Boltzmann population distribution (dependent upon the temperature of the molecular beam), are used to calculate the line strengths of the transitions. Solving the Schrödinger equation in a periodic potential has been well treated by Lewis et al.,[49] a brief description of their approach can be found in section S3.1.

4.3.1. Line Strengths. If the electronic transition dipole moment is assumed to be constant (with twist angle θ), then the transition intensity is proportional to the Franck−Condon factor (see section S3.2).[50] Due to the symmetry of the wave functions only even−even and odd−odd transitions occur. The populations of the ground-state potentials are calculated using a Boltzmann distribution corresponding to the temperature of the molecular beam. The relative line strength of a transition is given by the product of the separate modes' line strengths; this accounts for the relative populations and wave function overlaps of the different modes.

4.3.2. Band Shape Simulation. An initial attempt to simulate the band shape of an individual torsional transition with the rotational lines for a (nearly) prolate top gave a simulated band far narrower than that observed experimentally. The experimental band is assumed to be a combination of rotations and low-frequency nontorsional vibrational modes, and the band was successfully simulated using a pseudovibrational progression at each torsional line position, as shown in Figure 5. The constituent peak heights are given by a Boltzmann-like factor using a constant energy separation between the pseudovibrational transitions and a pseudotemperature, which is not the same as the torsional temperature. Each constituent peak is simulated by a mixed Gaussian and Lorentzian profile. The Gaussian character of the profiles, temperature, peak width and the energy separation of the pseudotransitions were altered to minimize

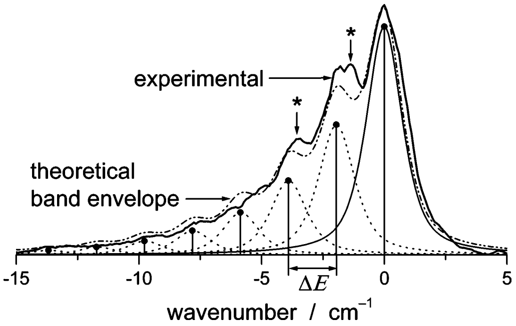

Figure 5. Simulation of the band shape of the 00 ← 00 torsional transition of BPEB using a pseudovibrational progression. The constituent Gaussian−Lorentzian profiles (dotted lines) are separated by the energy difference, ΔE, of the pseudovibrational transitions with peak heights (points) corresponding to a pseudo-Boltzmann distribution. The simulated envelope is shown with a dash−dotted line in comparison with the experiment (solid line). The stars (★) mark the position of hot-bands contributing to the experimental envelope.

the mean-square error between the simulation and the measured shape of the dominant 00 ← 00 ($v'_s v'_{as} \leftarrow v''_s v''_{as}$) transition.

4.4. Experimental Potentials. Although the largest peak in the spectrum can be assigned as the 00 ← 00 ($v'_s v'_{as} \leftarrow v''_s v''_{as}$) transition (which would have the highest population and the largest Franck−Condon factor and therefore the greatest line strength), assignment based on combination differences was ambiguous.

For the simulation of the spectra, a simple periodic potential of the form

$$V(\theta) = \frac{V_{max}}{2}(1 - \cos 2\theta) \qquad (2)$$

is used, where V_{max} is the barrier of the torsional potential and θ is the ring-to-ring torsional angle. V_{max} can be related to the force constant, k, of a harmonic potential, $V(\theta) = {}^1/_2 k\theta^2$, through the quadratic coefficient of the Taylor expansion of eq 2:

$$k = 2V_{max} \qquad (3)$$

The harmonic vibrational frequency, ν_e, is then given by

$$\nu_e = \frac{1}{2\pi}\sqrt{\frac{k}{I_{red}}} \qquad (4)$$

where I_{red} is the reduced moment of inertia (cf. Table 1 and see section S3.1). The two hot bands (to the left of the 00 ← 00 transition in Figure 3) are assumed to correspond to the 0 ← 2 transitions of the symmetric and antisymmetric modes. The hot band's separation from the 00 ← 00 origin, ΔE_{hb}, corresponds approximately to $2\nu_e$ (ignoring the anharmonicity) for each twisting mode. The following separations were obtained from the spectra: BPEB, $\Delta E^{as}_{hb} = 25.6$ cm^{-1} and $\Delta E^{s}_{hb} = 44.8$ cm^{-1}; D-BPEB, $\Delta E^{as}_{hb} = 25.6$ cm^{-1} and $\Delta E^{s}_{hb} = 42.2$ cm^{-1} (error approximately ± 0.05 cm^{-1}).

The approximate values for V_{max}, obtained via eqs 4 and 3, were optimized iteratively to minimize the mean-square error between the spectrum and the simulation, considering only the low-energy part including both hot bands and the 00 ← 00 transition. The experimentally determined torsional vibrational constants are $\nu^{as}_e = 13.00 \pm 0.05$ cm^{-1} and $\nu^{s}_e = 23.00 \pm 0.07$ cm^{-1}.

To simulate the whole spectrum, the excited-state potentials were assumed to be scaled versions of the ground-state potentials, with barrier heights $\approx 8V_{max}$, analogous to tolane.[35] The fit was optimized by varying the scaling factors of the excited states and the torsional temperature. The best fit parameters are summarized in Table 2.

The values of V_{max} obtained were 223 ± 2 cm^{-1} for the antisymmetric and 233 ± 2 cm^{-1} for the symmetric twist, which are close to the equivalent value of 202 cm^{-1} for tolane.[35] The barrier heights of both modes should be the same, as they correspond to the molecular energy at the fixed rotation angle of 90°. However, due to the low temperature in the molecular beam, only low-lying energy levels are sufficiently populated so that the experimental spectra are only sensitive to the bottom third of the ground-state potential. Consequently, V_{max} does not represent the true barrier height but defines the shape of the potential at the bottom. The corresponding torsional force constants are $k^{as} = 446$ cm^{-1} and $k^{s} = 466$ cm^{-1}. The difference in potential shapes is justified by the normal-mode analysis, which shows that the antisymmetric mode has an additional force constant for the next-nearest neighbor interaction, see Table 1. This can be understood as a difference in the long range π-interactions due to the differing orbital overlaps during the twisting motion of the two modes.

Following Table 1, the ring-to-ring and next-nearest neighbor torsional force constants are $k^{(1)} = k^{s} = 466$ cm^{-1} and $k^{(2)} = (k^{as} - k^{(1)})/2 = -9.9$ cm^{-1}, respectively.

Zheng et al. have studied the torsional motion of poly(phenylethynylene)s using Hartree−Fock self-consistent field theory.[38] The predicted vibrational constants for the antisymmetric mode, $\nu^{as}_e = 13.2$ cm^{-1}, is in very good agreement with experiment, whereas the value for the symmetric mode, $\nu^{s}_e = 19.4$ cm^{-1}, deviates significantly. On the basis of these theoretical values we derive force constants of $k^{(1)} = 324$ cm^{-1} and $k^{(2)} = 63$ cm^{-1} for the ring-to-ring and next-nearest neighbor interactions, respectively, which are in stark contrast with the experimental values of this study.

4.5. Simulation and Spectral Assignment. It was now possible to assign the BPEB spectrum using the simulation, Figure 6a. Furthermore, the D-BPEB spectrum was assigned by changing only the inertia of the inner ring in the simulation program, Figure 6b. The parameters used to simulate both spectra are given in Table 2.

The simulated torsional progressions fit the early parts of both spectra very well but do not fully describe the experimental spectra at higher wavenumbers; see also Supporting Information section S3.3. Additional torsional progressions were required to simulate the missing intensity; their properties are listed in Table 2. Their positions are indicated by combs and their intensities are included in the simulations in Figure 6. These extra torsional progressions may originate from other low-frequency vibrational modes.

The full simulation shows that the peak positions are very well reproduced, and the peak intensities reasonably well (Figure 6). Experimental intensities may be inaccurate due to the instability of the nozzle during the scan, which resulted in changing beam density and temperature.

The absolute line positions (including air-to-vacuum corrections and the calibration of the dye laser wavelength) of the 00 ← 00 band origins have been determined as 31 269.7 ± 0.5 cm^{-1} for BPEB and 31 297.1 ± 0.5 cm^{-1} for D-BPEB.

5. DFT Potentials

An initial approach to the problem of assigning the large number of transitions in the BPEB spectrum (Figure 3) was to use computational methods to calculate the torsional potentials.

Density functional theory (DFT) calculations were carried out using the Gaussian 98 package[51] with Pople's 6-31G basis

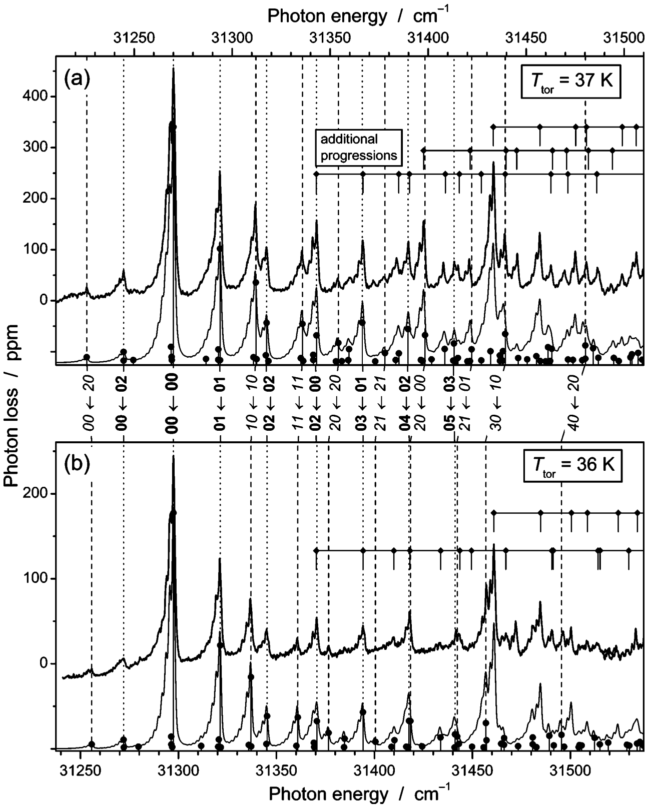

Figure 6. Comparison of experimental (upper traces) and simulated (lower traces) spectra for BPEB (a) and D-BPEB (b). The transitions of the main torsional progression are shown as vertical sticks with intensities shown by points. The most intense transitions of the main torsional progression are labeled between the panels ($v'_s v'_{as} \leftarrow v''_s v''_{as}$). Key: bold labels, pure antisymmetric transitions (dotted vertical lines); italic labels, transitions with symmetric contributions (dashed vertical lines). The locations of additional torsional progressions originating from other vibrational modes are shown with combs starting at the position of the 00 ← 00 transition (see text).

set supplemented by one d-function on heavy atoms and p-polarization functions on the hydrogens and with (and without) additional diffuse functions on the heavy atoms. The DFT calculations were carried out using Becke's three-parameter hybrid exchange functional[52] with Lee−Yang−Parr gradient-corrected correlation functional (B3LYP).[53]

5.1. Ground State. The fully optimized geometry of the ground state of BPEB was determined using B3LYP/6-31G** with no constraints on bond lengths, angles or dihedral angles. The results are listed in comparison with X-ray single-crystal data[54] in the Supporting Information (Table 1S). The optimized geometry was found to be planar with D_{2h} symmetry.

The moments of inertia required for the spectral analysis were obtained from this B3LYP/6-31G** optimized geometry and are listed in Table 2. The torsional potentials of BPEB in the symmetric and antisymmetric modes were obtained with further calculations at the B3LYP/6-31G** level of theory. The geometry was again allowed to fully optimize, apart from the ring-to-ring dihedral angle which was fixed according to a grid of points over the torsional angle, θ. An angular grid with 5° spacing was used up to 70° with additional points at 0.1°, 1°, 3°, 80° and 90°. The $\theta = 0°$ geometry point was excluded as its energy is 6.26 cm^{-1} below the energy of the 0.1° geometry, which is believed to be an artifact of the calculation methodology. The ground-state torsional potentials are shown in the Supporting Information (Figure 5S).

Allowing all parameters but the torsional angle to optimize shows that the ring-to-ring distance increases by 0.0092 Å (or 0.2%) on twisting from 0° to 90°. No evidence was found for a ring breathing mode being coupled with the twisting modes (the largest ring carbon−carbon bond length change was 0.1% from planar to perpendicular geometry), as suggested by Zheng et al.[38]

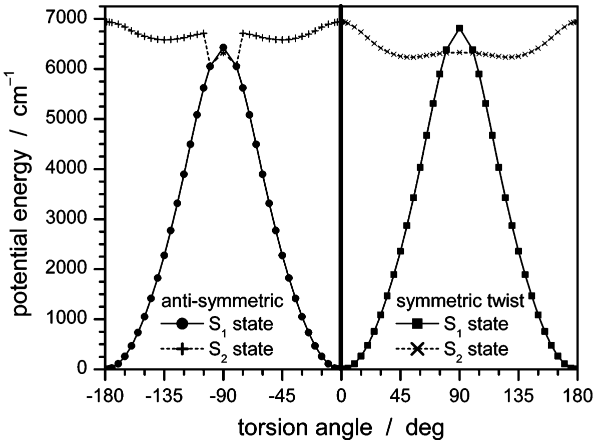

Figure 7. First two singlet excited states of BPEB, symmetric and antisymmetric torsional potentials. Calculated DFT points are connected by straight lines.

5.2. Excited State. The optimized geometries of the ground state at each twisting angle were used to calculate the energies required to excite the molecule to the lowest three singlet excited states. The calculations were carried out using the time-dependent DFT (TD-DFT) methodology[55−57] at the B3LYP/6-31G** level of theory.

The excitation energy plus the ground-state energy allowed the calculation of torsional potentials for the first two singlet excited states, S$_1$ and S$_2$ (shown in Figure 7). An interesting observation is the true/avoided crossing of these two states at around 80° which will affect the energy levels at the top of the torsional barrier of the S$_1$ state. The Gaussian program failed to determine the symmetry of the excited states; thus, the nature of the crossing (true or avoided) could not be ascertained. The S$_2$ state has a local maximum at its planar geometry, and minima at 35° and 25° for the symmetric and antisymmetric twists, respectively (see Figure 7). The spectroscopy of the second excited state is therefore expected to be markedly different to the current study.

The bottom of the S$_1$ potentials are approximately 8 times as steep as the ground-state potentials and follow closely the cosine form of eq 2. Using fluorescence spectroscopy, Okuyama et al. have determined a very similar scaling factor of 8 for tolane.[35] At higher energies, not accessed in the current study, the S$_1$ potentials deviate significantly from eq 2. In addition, the true barrier height of the S$_1$ potential cannot be derived due to the uncertainty caused by the crossing of the S$_1$ and S$_2$ states.

5.3. Simulation Using DFT Potentials. A simulation based on spline fits to the DFT potentials failed to match the experimental spectrum. The DFT ground-state torsional barrier of BPEB (731 cm^{-1}) is over 3 times that of our experimentally derived barrier (230 cm^{-1}), and over 3.5 times that of tolane (202 cm^{-1} [35]). Though a slight increase in barrier height can be justified by the extended π-conjugation in BPEB, a 350% gain is extreme compared with the 14% gain observed experimentally. The extremely poor fit of the spectrum and the comparison with experimentally derived barriers led to the conclusion that the DFT derived potentials cannot be used to describe the torsional motions of BPEB. The failure of the DFT potential may be due to numerical inaccuracies imposed by computational limitations, or due to the inability of current exchange functionals to describe π-bond breaking effects experienced by conjugated molecules undergoing torsional motion.[58]

6. Conclusions

High-resolution absorption spectra of jet-cooled BPEB have been measured in the first UV absorption band. Individual torsional transitions within the $\pi^* \leftarrow \pi$ electronic transition were resolved. Spectral lines resulting from the symmetric twisting mode were identified by isotopic substitution of the hydrogens on the central ring (D-BPEB). BPEB and D-BPEB torsional spectra were successfully simulated using simple periodic potentials (eq 2) based on the experimentally determined torsional vibrational frequencies of $\nu_e^{as} = 13.00 \pm 0.05$ cm^{-1} and $\nu_e^{s} = 23.00 \pm 0.07$ cm^{-1}.

The experimentally determined ground-state torsional potentials are in stark contrast to the results from DFT calculations, which overestimate the measured barrier height significantly. It has been suggested that current exchange functionals fail to describe π-bond breaking effects of extended conjugated molecules undergoing torsional motion.[58] Additionally, numerical inaccuracies imposed by computational limitations may have prevented DFT from producing an accurate potential. Nevertheless, the shapes of the DFT ground-state potentials show only small deviations from the simple, periodic cosine potential (see section S4.2). For the excited states, the DFT calculations suggest a true/avoided crossing between S_1 and S_2 near the maximum of the torsion potentials of the S_1 state (Figure 7). S_2 has a local maximum at its planar geometry and its spectroscopy is expected to be markedly different compared to the S_1 state studied in this work.

The difference between the shapes of the symmetric and antisymmetric potentials at small torsional angles, found in both the experimental and DFT potentials, is rationalized by the different long range π-interactions of the two modes. The experimentally derived ring-to-ring and next-nearest neighbor torsional force constants are $k^{(1)} = 466$ cm^{-1} and $k^{(2)} = -9.9$ cm^{-1}, respectively.

The analysis of the spectra allowed the first experimental determination of the torsional barrier height of BPEB. Although, due to the low temperature in the molecular beam, this barrier height could only be estimated to be 220−235 cm^{-1}, which is slightly higher than the equivalent value of 202 cm^{-1} for tolane.[35] The similarity of these values indicate that the additional long-range π-conjugation in the three ring system, BPEB, has a small additional stiffening effect on the torsional motion.

The torsional barrier height of BPEB ($\approx$230 or $\approx$2.7 kJ mol^{-1}) is comparable with kT at room temperature (207 cm^{-1}), thus, at ambient temperature 30% of BPEB molecules in a sample will have sufficient energy to allow the “free” rotation of the phenyl rings. This finding highlights the difficulties encountered by conductance studies in decoupling the role of electron hopping and through conjugation on the transport properties of molecular wires. In a recent theoretical study of molecular wires, Berlin et al. have shown that the electon/hole mobility is crucially affected by the conformational changes caused by the twisting and rotational motions of the aromatic rings,[59] making the prediction of the transport properties nontrivial. To study the effect of through conjugation in isolation, more conformational control of the ground-state geometry is required, e.g., by substitution to increase the depths of the torsional ground-state potential. Studies to this end are in progress.

Acknowledgment. We thank M. N. R. Ashfold, A. J. Orr-Ewing, C. M. Western and the Laser Chemistry, Spectroscopy and Dynamics Group at the University of Bristol for vacuum equipment, UV cavity-mirrors, the WI2 simulation program and many helpful discussions about cavity ring-down spectroscopy. We also thank J. P. Simons and L. C. Snoek (Oxford) for the oven design. S. J. Greaves and E. L. Flynn acknowledge the funding of studentships by EPSRC and the Department of Chemistry, University of Durham. We also acknowledge the assistance of N. Elliot and V. L. Whittle in the early stages of the experimental development, and the mechanical and electrical workshops of the Chemistry Department in Durham. We thank the EPSRC and One North East (UIC Nanotechnology) for financial support.

Supporting Information Available: Some additional detail of the vacuum chamber is given and a method to optimize the placement of the coupling lens in front of the cavity is described. The preparation of 1,4-bis(phenylethynyl)-2,3,5,6-tetradeuteriobenzene is described in detail. The normal-mode analysis is detailed along with a description of the treatment of the Schrödinger equation in a periodic potential. An additional comparison between the experimental and simulated spectra of BPEB is presented. The results of the DFT calculations of the ground-state torsional potential are presented including a comparison of the ground-state optimized geometry with X-ray crystal data. This material is available free of charge via the Internet at http://pubs.acs.org.

References and Notes

(1) Schwab, P. F. H.; Levin, M. D.; Michl, J. *Chem. Rev.* **1999**, *99*, 1863−1933.

(2) Bunz, U. H. F. *Chem. Rev.* **2000**, *100* (4), 1605−1644.

(3) Moore, J. S. *Acc. Chem. Res.* **1997**, *30*, 402−413.

(4) Levitsky, I. A.; Kim, J. S.; Swager, T. M. *J. Am. Chem. Soc.* **1999**, *121* (7), 1466−1472.

(5) Kim, K.; Webster, S.; Levi, N.; Carroll, D. L.; Pinto, M. R.; Schanze, K. S. *Langmuir* **2005**, *21* (11), 5207−5211.

(6) Ding, L.; Lu, Z.; Egbe, D. A. M.; Karasz, F. E. *Macromol.* **2004**, *37* (26), 10031−10035.

(7) Arias-Marin, E.; Arnault, J. C.; Guillon, D.; Maillou, T.; Moigne, J.; Geoffroy, B.; Nunzi, J. M. *Langmuir* **2000**, *16* (9), 4309−4318.

(8) Roy, V. A. L.; Zhi, Y. G.; Zu, Z. X.; Yu, S. C.; Chan, P. W. H.; Che, C. M. *Adv. Mater.* **2005**, *17* (10), 1258−1261.

(9) Erdogan, B.; Song, L.; Wilson, J. N.; Park, J. O.; Srinivasarao, M.; Bunz, U. H. F. *J. Am. Chem. Soc.* **2004**, *126* (12), 3678−3679.

(10) Ward, M. D. *J. Chem. Educ.* **2001**, *78* (3), 321−328.

(11) James, D. K.; Tour, J. M. *Chem. Mater.* **2004**, *16* (23), 4423−4435.

(12) Reichert, J.; Ochs, R.; Beckmann, D.; Weber, H. B.; Mayor, M.; v. Lhneysen, H. *Phys. Rev. Lett.* **2002**, *88* (17), 176804.

(13) Bumm, L. A.; Arnold, J. J.; Cygan, M. T.; Dunbar, T. D.; Burgin, T. P.; Jones, L., II; Allara, D. L.; Tour, J. M.; Weiss, P. S. *Science* **1996**, *271* (5256), 1705−1707.

(14) Creager, S.; Yu, C. J.; Bamdad, C.; O’Connor, S.; MacLean, T.; Lam, E.; Chong, Y.; Olsen, G. T.; Luo, J.; Gozin, M.; Kayyem, J. F. *J. Am. Chem. Soc.* **1999**, *121* (5), 1059−1064.

(15) Donhauser, Z. J.; Mantooth, B. A.; Kelly, K. F.; Bumm, L. A.; Monnell, J. D.; Stapleton, J. J.; Price, D. W., Jr.; Rawlett, A. M.; Allara, D. L.; Tour, J. M.; Weiss, P. S. *Science* **2001**, *292*, 2303−2307.

(16) Chen, J.; Reed, M. A.; Rawlett, A. M.; Tour, J. M. *Science* **1999**, *286*, 1550−1552.

(17) Chen, J.; Wang, W.; Reed, M. A.; Rawlett, A. M.; Price, D. W.; Tour, J. M. *Appl. Phys. Lett.* **2000**, *77*(8), 1224−1226.

(18) Seminario, J. M.; Derosa, P. A.; Bastos, J. L. *J. Am. Chem. Soc.* **2002**, *124* (35), 10266−10267.

(19) Lewis, P. A.; Inman, C. E.; Yao, Y.; Tour, J. M.; Hutchison, J. E.; Weiss, P. S. *J. Am. Chem. Soc.* **2004**, *126* (39), 12214−12215.

(20) Majumder, C.; Briere, T.; Mizuseki, H.; Kawazoe, Y. *J. Phys. Chem. A* **2002**, *106* (34), 7911−7914.

(21) Donhauser, Z. J.; Mantooth, B. A.; Pearl, T. P.; Kelly, K. F. *Jpn. J. Appl. Phys. Pt. 0* **2002**, *41* (7B), 4871−4877.

(22) Karzazi, Y.; Cornil, J.; Brédas, J. L. *Nanotechnology* **2003**, *14* (2), 165−171.

(23) Khondaker, S.; Yao, Z.; Cheng, L.; Henderson, J.; Yao, Y.; Tour, J. *Appl. Phys. Lett.* **2004**, *85* (4), 645−647.

(24) Majumber, C.; Mizuseki, H.; Kawazoe, Y. *J. Mol. Struct. (THEOCHEM)* **2004**, *681* (1−3), 65−69.

(25) Seminario, J. M.; Zacarias, A. G.; Tour, J. M. *J. Am. Chem. Soc.* **2000**, *122* (13), 3015−3020.

(26) Levitus, M.; Schmieder, K.; Ricks, H.; Shimizu, K. D.; Bunz, U. H. F.; Garcia-Garibay, M. A. *J. Am. Chem. Soc.* **2001**, *123* (18), 4259−4265.

(27) Tomfohr, J.; Sankey, O. F. *J. Chem. Phys.* **2004**, *120* (3), 1542−1554.

(28) Brizius, G.; Billingsley, K.; Smith, M. D.; Bunz, U. H. F. *Org. Lett.* **2003**, *5* (21), 3951−3954.

(29) Crisp, G. T.; Bubner, T. P. *Tetrahedron* **1997**, *53* (34), 11881−11898.

(30) Crisp, G. T.; Bubner, T. P. *Tetrahedron* **1997**, *53* (34), 11899−11912.

(31) Benniston, A. C.; Harriman, A.; Li, P.; Sams, C. A.; Ward, M. D. *J. Am. Chem. Soc.* **2004**, *126* (42), 13630−13631.

(32) Benniston, A. C.; Harriman, A.; Li, P.; Sams, C. A. *J. Am. Chem. Soc.* **2005**, *127* (8), 2553−2564.

(33) Beeby, A.; Findlay, K.; Low, P. J.; Marder, T. B. *J. Am. Chem. Soc.* **2002**, *124* (28), 8280−8284.

(34) Beeby, A.; Findlay, K.; Low, P. J.; Marder, T. B.; Matousek, P.; Parker, A. W.; Rutter, S. R.; Towrie, M. *Chem. Commun.* **2003**, No. 19, 2406−2407.

(35) Okuyama, K.; Hasegawa, T.; Ito, M.; Mikami, N. *J. Phys. Chem.* **1984**, *88* (9), 1711−1716.

(36) Okuyama, K.; Cockett, M. C. R.; Kimura, K. *J. Chem. Phys.* **1992**, *97* (3), 1649−1654.

(37) Ishibashi, T.; Hamaguchi, H. *J. Phys. Chem. A* **1998**, *102* (13), 2263−2269.

(38) Zheng, X.; Vedova-Brook, N.; Sohlberg, K. *J. Phys. Chem. A* **2004**, *108* (13), 2499−2507.

(39) Snoek, L. C.; Robertson, E. G.; Kroemer, R. T.; Simons, J. P. *Chem. Phys. Lett.* **2000**, *321*, 49−56.

(40) Sample oven design. Simons, J. P.; Snoek, L. C. Private communication.

(41) Hillenkamp, M.; Keinan, S.; Even, U. *J. Chem. Phys.* **2003**, *118* (19), 8699−8705.

(42) O'Keefe, A.; Deacon, D. A. G. *Rev. Sci. Instrum.* **1988**, *59* (12), 2544−2551.

(43) Wheeler, M. D.; Newman, S. M.; Orr-Ewing, A. J.; Ashfold, M. N. R. *J. Chem. Soc., Faraday Trans.* **1998**, *94* (3), 337−351.

(44) Vallance, C. *New J. Chem.* **2005**, *29* (7), 867−874.

(45) Lee, D. H.; Yoon, Y.; Kim, B.; Lee, J. Y.; Yoo, Y. S.; Hahn, J. W. *Appl. Phys. B* **2002**, *74* (4−5), 435−440.

(46) CRDS LabVIEW program. Orr-Ewing, A. J.; Rennick, C. J. Private communication.

(47) Lydon, D. P.; Porrès, L.; Beeby, A.; Marder, T. B.; Low, P. J. *New J. Chem.* **2005**, *29* (7), 972−976.

(48) WI2 simulation program for molecular iodine spectra. Western, C. M. Private communication.

(49) Lewis, J. D.; Malloy, T. B.; Chao, T. H.; Laane, J. *J. Mol. Struct.* **1971**, *12* (3), 427−449.

(50) Bernath, P. F. *Spectra of Atoms and Molecules*; Oxford University Press: Oxford, U.K., 1995.

(51) Frisch, M. J.; Trucks, G. W.; Schlegel, H. B.; Scuseria, G. E.; Robb, M. A.; Cheeseman, J. R.; Zakrzewski, V. G.; Montgomery, J. A., Jr..; Stratmann, R. E.; Burant, J. C.; Dapprich, S.; Millam, J. M.; Daniels, A. D.; Kudin, K. N.; Strain, M. C.; Farkas, O.; Tomasi, J.; Barone, V.; Cossi, M.; Cammi, R.; Mennucci, B.; Pomelli, C.; Adamo, C.; Clifford, S.; Ochterski, J.; Petersson, G. A.; Ayala, P. Y.; Cui, Q.; Morokuma, K.; Malick, D. K.; Rabuck, A. D.; Raghavachari, K.; Foresman, J. B.; Cioslowski, J.; Ortiz, J. V.; Baboul, A. G.; Stefanov, B. B.; Liu, G.; Liashenko, A.; Piskorz, P.; Komaromi, I.; Gomperts, R.; Martin, R. L.; Fox, D. J.; Keith, T.; Al-Laham, M. A.; Peng, C. Y.; Nanayakkara, A.; Challacombe, M.; Gill, P. M. W.; Johnson, B.; Chen, W.; Wong, M. W.; Andres, J. L.; Gonzalez, C.; Head-Gordon, M.; Replogle, E. S.; Pople, J. A. *Gaussian 98*, revision a.9; Gaussian, Inc.: Pittsburgh, PA, 1998.

(52) Becke, A. D. *J. Chem. Phys.* **1993**, *98*, 5648−5652.

(53) Lee, C.; Yang, W.; Parr, R. G. *Phys. Rev. B* **1988**, *37*, 785−786.

(54) Zhao, L.; Perepichka, I. F.; Türksoy, F.; Batsanov, A. S.; Beeby, A.; Findlay, K.; Bryce, M. R. *New. J. Chem.* **2004**, *28*, 912−918.

(55) Stratmann, R. E.; Scuseria, G. E.; Frisch, M. J. *J. Chem. Phys.* **1998**, *109*, 8218−8224.

(56) Bauernschmitt, R.; Ahlrichs, R. *Chem. Phys. Lett.* **1996**, *256*, 454−460.

(57) Casida, M. E.; Jamorski, C.; Casida, K. C.; Salahub, D. R. *J. Chem. Phys.* **1998**, *108*, 4439−4449.

(58) Sancho-Garcia, J. C.; Cornil, J. *J. Chem. Phys.* **2004**, *121*, 3096−3101.

(59) Berlin, Y. A.; Hutchison, G. R.; Rempala, P.; Ratner, M. A.; Michl, J. *J. Phys. Chem. A* **2003**, *107* (19), 3970−3980.